The EMBO Journal (2012) 31, 3309–3322 | © 2012 European Molecular Biology Organization | All Rights Reserved 0261-4189/12
www.embojournal.org

THE EMBO JOURNAL

The F-BAR protein NOSTRIN participates in FGF signal transduction and vascular development

Igor Kovacevic[1], Jiong Hu[2], Ann Siehoff-Icking[1], Nils Opitz[1], Aliesha Griffin[3], Andrew C Perkins[3], Alan L Munn[3,4], Werner Müller-Esterl[1], Rüdiger Popp[2], Ingrid Fleming[2], Benno Jungblut[5], Meike Hoffmeister[1] and Stefanie Oess[1,*]

[1]Institute for Biochemistry II, Goethe University Frankfurt Medical School, Frankfurt/Main, Germany, [2]Institute for Vascular Signalling, Goethe University Frankfurt Medical School, Frankfurt/Main, Germany, [3]Institute for Molecular Bioscience, The University of Queensland, Brisbane, Queensland, Australia, [4]School of Medical Science and Molecular Basis of Disease Program, Griffith Health Institute, Griffith University (Gold Coast), Southport, Queensland, Australia and [5]Department of Cardiac Development and Remodeling, Max Planck Institute for Heart and Lung Research, Bad Nauheim, Germany

F-BAR proteins are multivalent adaptors that link plasma membrane and cytoskeleton and coordinate cellular processes such as membrane protrusion and migration. Yet, little is known about the function of F-BAR proteins *in vivo*. Here we report, that the F-BAR protein NOSTRIN is necessary for proper vascular development in zebrafish and postnatal retinal angiogenesis in mice. The loss of NOSTRIN impacts on the migration of endothelial tip cells and leads to a reduction of tip cell filopodia number and length. NOSTRIN forms a complex with the GTPase Rac1 and its exchange factor Sos1 and overexpression of NOSTRIN in cells induces Rac1 activation. Furthermore, NOSTRIN is required for fibroblast growth factor 2 dependent activation of Rac1 in primary endothelial cells and the angiogenic response to fibroblast growth factor 2 in the *in vivo* matrigel plug assay. We propose a novel regulatory circuit, in which NOSTRIN assembles a signalling complex containing FGFR1, Rac1 and Sos1 thereby facilitating the activation of Rac1 in endothelial cells during developmental angiogenesis.

The EMBO Journal (2012) **31,** 3309–3322. doi:10.1038/emboj.2012.176; Published online 29 June 2012
Subject Categories: signal transduction; development
Keywords: angiogenesis; F-BAR protein; FGF signal transduction; Rac1; tip cell

Introduction

Developmental angiogenesis is a highly stereotypical process, leading to the establishment of organ-specific vascular branching patterns with reproducible anatomy (Larrivee *et al*, 2009). These are formed by angiogenic sprouts, which consist of several types of specialised endothelial cells. Tip cells are located at the leading position of the vascular sprout. They form numerous cellular protrusions, referred to as filopodia (Gerhardt *et al*, 2003), which constantly sense the microenvironment for guidance cues to navigate the growing vessel. Tip cells also regulate capillary branching by detecting and connecting to neighbouring sprouts. Stalk cells follow the leading tip cell; they proliferate and thereby elongate the growing branch (Gerhardt *et al*, 2003; De Smet *et al*, 2009; Larrivee *et al*, 2009). The assignment of these specialised functions, however, is only transient and endothelial cells dynamically shuffle their relative positioning in the angiogenic sprout (Jakobsson *et al*, 2010), probably due to continuous competition for the tip cell function. Finally quiescent phalanx cells build the inner lining of the new vessel after its outline has been set. (Gerhardt *et al*, 2003; De Smet *et al*, 2009; Larrivee *et al*, 2009).

Several attractive and repellent guidance cues and their respective receptors are known, which direct the migration of the developing blood vessel. Many of these are shared between the vascular and the neural system, such as Slits/Robo receptors and Netrins/Unc5. Moreover, growth factors such as VEGF and FGF, are key regulators of vascular development, through the stimulation of directed migration and proliferation of endothelial cells (Gerhardt *et al*, 2003; Gerhardt and Betsholtz, 2005; Horowitz and Simons, 2008; De Smet *et al*, 2009; Larrivee *et al*, 2009). The sensing of the directional cues through filopodia as well as their translation into directed migration strongly depend on coordination of the tip cell cytoskeleton with membrane dynamics (Suchting *et al*, 2006; De Smet *et al*, 2009). Tip cells are highly polarised and the formation of lamellipodia and filopodia is one key characteristic. The activity of small GTPases is thought to be essential for tip cell function, however comparatively little is known about the factors that control cytoskeleton dynamics and small GTPase activity in the context of tip cell protrusion formation and migration (Tan *et al*, 2008; De Smet *et al*, 2009; Wang *et al*, 2010).

Recently F-BAR (Fes/CIP4 homology and Bin/amphiphysin/Rvs) proteins have emerged as important regulators of cell protrusion formation and migration as well as endocytosis. These processes require the concerted action of the plasma membrane and the cytoskeleton and F-BAR proteins are modular molecules that serve as multivalent adaptors that physically and functionally link both compartments. They comprise a common N-terminal F-BAR domain followed by various combinations of kinase, SH2, SH3 and GTPase interacting domains. The F-BAR domain senses and shapes membrane curvature, while a majority of F-BAR proteins uses the C-terminal domains to interact with components and regulators of the actin cytoskeleton, e.g. actin nucleation promoting factors WASP and N-WASP, Arp2/3 and the large GTPase dynamin (Heath and Insall, 2008; Frost *et al*, 2009; Roberts-Galbraith and Gould, 2010; Suetsugu *et al*, 2010; Qualmann *et al*, 2011).

*Corresponding author. Institute for Biochemistry II, Goethe University Frankfurt Medical School, Theodor Stern Kai 7 Hs 75, 60590 Frankfurt/Main, Germany. Tel.: +49 69 6301 5820; Fax: +49 69 6301 5577; E-mail: oess@biochem2.de

Received: 2 February 2012; accepted: 1 June 2012; published online: 29 June 2012

The F-BAR protein NOSTRIN was identified by our group as modulator of the subcellular localisation and activity of endothelial nitric oxide synthase (eNOS) and was hence termed eNOS traffic inducer (Zimmermann *et al*, 2002; Oess *et al*, 2006; Schilling *et al*, 2006; McCormick *et al*, 2011). NOSTRIN associates with membranes via its F-BAR domain (Icking *et al*, 2006) and binds dynamin and N-WASP through its C-terminal SH3 domain. Like other F-BAR proteins, NOSTRIN forms oligomers and hence allows simultaneous interaction with several SH3 binding partners, thereby coordinating the function of dynamin and N-WASP to facilitate the endocytosis of eNOS (Icking *et al*, 2005).

For many F-BAR proteins the physiological function *in vivo* is unclear. In this study we report an important role for the F-BAR protein NOSTRIN in developmental angiogenesis and identify the molecular mechanisms by which NOSTRIN links FGFR1 with the activation of the GTPase Rac1.

Results

The knockdown of NOSTRIN in developing zebrafish embryos causes vascular defects

NOSTRIN shows the highest expression in endothelial cells and highly vascularised organs (Zimmermann *et al*, 2002). To study the *in vivo* function of NOSTRIN in the vascular system, we have chosen developing zebrafish as a model, due to their *ex utero* development, the transparency of early embryos and the availability of transgenic strains *Tg(fli1a:EGFP)^{y1}* and *Tg(kdrl:EGFP)^{s843}* with endothelial cell-specific expression of eGFP (Lawson and Weinstein, 2002; Jin *et al*, 2005). We carried out an antisense morpholino oligonucleotide (MO)-mediated knockdown (KD) of NOSTRIN in developing *Tg(fli1a:EGFP)^{y1}* or *Tg(kdrl:EGFP)^{s843}* zebrafish, using two different MO directed against the translational start ATG (ATG MO) or the splice site inside the sequence coding for the SH3 domain (Splice MO). Zebrafish embryos injected with the NOSTRIN-targeting MO (referred to as morphants) did not show lethality or gross morphological changes during the period of inspection up to 72 hpf when compared to wildtype (WT) or Control MO-injected embryos, with the exception of axis defects in a small subset (1%) of morphants (Figure 1A and B).

However, the NOSTRIN morphants displayed oedema and haemorrhaging e.g. in the hindbrain and pericardial regions, indicative of a malfunctioning vascular system (Figure 1A, B and E). Analysing the developing vasculature, an abnormal trajectory phenotype of intersegmental vessels (ISV), with improper connections formed between neighbouring ISVs in both morphants was observed. Moreover, the dorsal longitudinal anastomotic vessels (DLAV) were misshaped or interrupted and the caudal artery (CA) and caudal vein plexus (CVP) were irregular in appearance (Figure 1C). In addition, we have found that KD of NOSTRIN leads to an impaired subintestinal vein (SIV) development (Supplementary Figure S1). The specificity of the vascular defects was demonstrated by a dose-dependent rescue of the phenotype by re-introduction of NOSTRIN by sequential injection of zebrafish NOSTRIN mRNA in combination with the Splice MO (Figure 1C and E, Supplementary Figure S1). KD efficiency and expression of NOSTRIN after mRNA injection were verified by immunoblotting (Figure 1D). These observations indicated an essential role of NOSTRIN for proper vascular development in zebrafish.

NOSTRIN morphants show an abnormal ISV trajectory phenotype associated with altered tip cell morphology and filopodia length

In order to analyse the development of the ISVs in more detail, we performed *in vivo* time-lapse microscopy of NOSTRIN morphants (Figure 2A, images extracted from Supplementary Videos 1 and 2). In WT embryos, the first ISVs to originate as sprouts from the DA were visible at 20–24 hpf, grew dorsally and reached the level of the top of the neural tube at approximately 30 hpf. They bifurcated to form 2 branches extending in a T-shaped fashion along the body axis, finally joining up to form the DLAV at 32–36 hpf (Figure 2A, left and Supplementary Video 1). In contrast, in NOSTRIN morphants the ISV sprouts appeared later at approximately 24–28 hpf and failed to establish the regular ISV trajectory but formed connections with neighbouring ISVs before reaching the top of the neural tube (Figure 2A, right and Supplementary Video 2). Therefore we conclude that NOSTRIN is important for the formation and/or the directed movement of ISV sprouts.

To determine whether this ISV defect was associated with a change in endothelial tip cell morphology, we analysed the tip cells of growing ISVs by confocal laser scanning microscopy (CLSM) and found that in WT embryos the tip cells exhibited the characteristic elongated shape (Wang *et al*, 2010; Yu *et al*, 2010) with long filopodial extensions (15.8% of filopodia/cell $>15\,\mu m$, 21.6% $<5\,\mu m$). In contrast, the tip cells in morphants were stub-like and exhibited significantly shorter filopodial extensions (1.1% $>15\,\mu m$, 42.3% $<5\,\mu m$; Figure 2B and C for full quantification). This suggests that NOSTRIN is critical for endothelial tip cell function, especially for filopodia formation, and that tip cell defects might cause the observed deviation from the stereotypical developmental pattern in the NOSTRIN morphants.

Postnatal retinal angiogenesis is impaired in NOSTRIN knockout mice

To further study the importance of NOSTRIN for tip cell function *in vivo*, we analysed postnatal retinal angiogenesis (Gerhardt *et al*, 2003) in NOSTRIN knockout (KO) mice. NOSTRIN KO mice were generated by loss-of-function genetics (Methods and Supplementary Figure S2) and will be described in detail independently of this study. In NOSTRIN KO mice the stereotypical spreading of the primary vascular plexus from the optic disc to the peripheral margin of the retina was impaired, measured as reduction of the mean vascular radius (Figure 3A and B) and the vascularised area of the retina at postnatal day (P)2, P5 and P7 (Figure 3A and C). In accordance, the number of branch points at the vascular front and the central region of the retina was significantly decreased in NOSTRIN KO mice at P5 (Figure 3D). Importantly, the guiding neuronal network comprising the pre-existing astrocyte scaffold was not altered in NOSTRIN KO retinas (Supplementary Figure S3). These findings suggest an impairment of the angiogenic capacity of endothelial cells, that in general is determined i.a. by endothelial cell proliferation and migration (Larrivee *et al*, 2009). Indeed, proliferation was reduced in retinas of NOSTRIN KO mice, measured as the number of phospho-Histone H3- (Figure 3G and H) or ki67- positive endothelial cell nuclei in the vascular front (Supplementary Figure S4). Detailed analysis of the tip cells revealed, that the number of

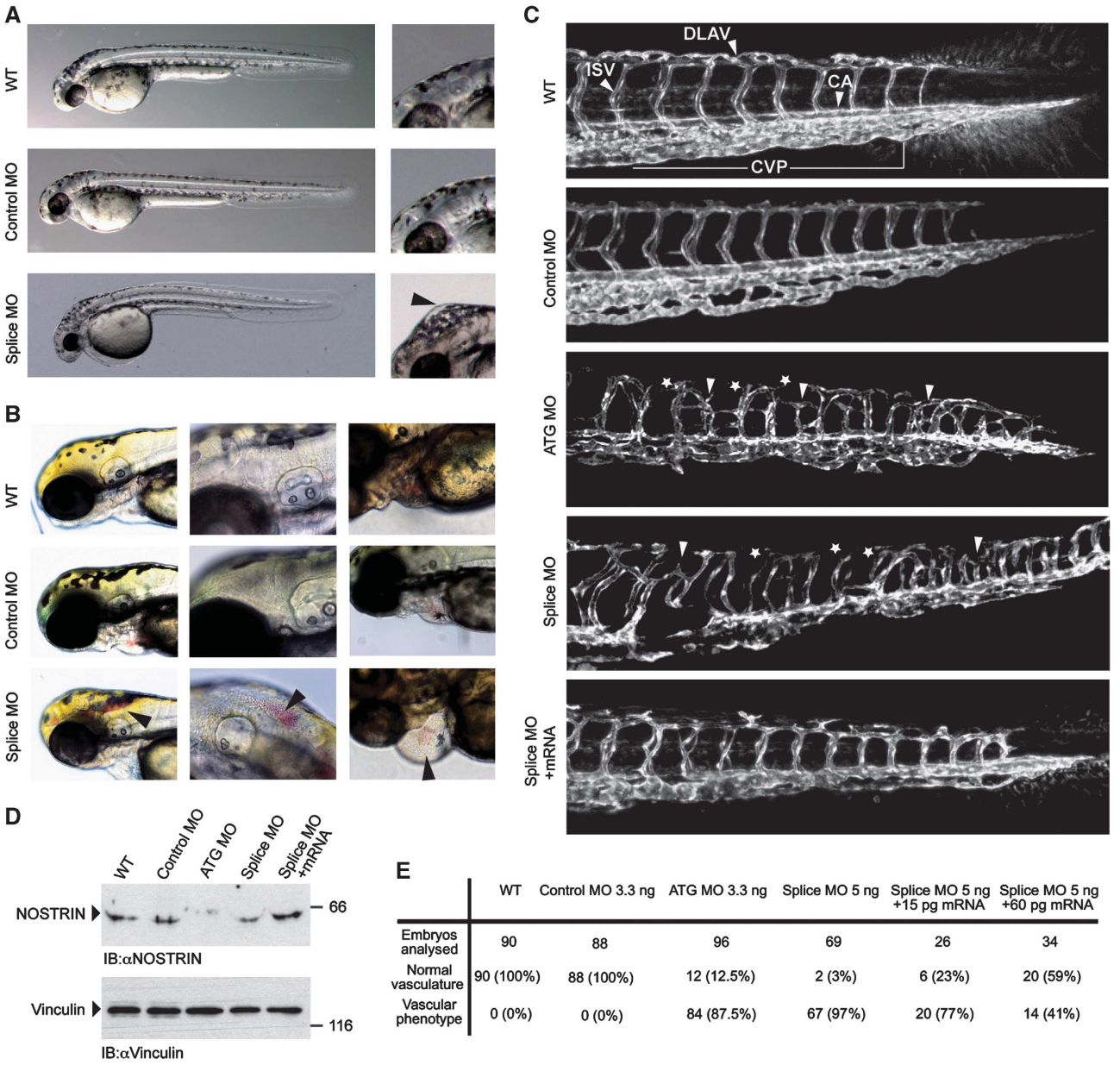

E

	WT	Control MO 3.3 ng	ATG MO 3.3 ng	Splice MO 5 ng	Splice MO 5 ng +15 pg mRNA	Splice MO 5 ng +60 pg mRNA
Embryos analysed	90	88	96	69	26	34
Normal vasculature	90 (100%)	88 (100%)	12 (12.5%)	2 (3%)	6 (23%)	20 (59%)
Vascular phenotype	0 (0%)	0 (0%)	84 (87.5%)	67 (97%)	20 (77%)	14 (41%)

Figure 1 MO-mediated KD of NOSTRIN in developing zebrafish embryos causes vascular defects. *Tg(fli1a:EGFP)*^{y1} zebrafish embryos were injected with 3.3 ng Control MO, 3.3 ng ATG MO, 5 ng Splice MO or 15 pg zebrafish NOSTRIN mRNA, if not indicated otherwise. All zebrafish images are lateral views with the anterior to the left and the dorsal side up. (**A**) Development of NOSTRIN morphants. Embryos injected with the Splice MO showed an overall regular development at 48 hpf when compared to WT embryos or embryos injected with Control MO (left). Higher magnification of embryo heads, black arrowhead pointing to hindbrain oedema in embryo injected with the Splice MO (right). (**B**) Cranial haemorrhaging (left and middle) and pericardial oedema and haemorrhaging (right) in embryos injected with the Splice MO analysed at 72 hpf, black arrowheads indicating red blood cells. (**C**) CLSM images of trunk regions taken at 48 hpf, with the vascular structures visualised by eGFP fluorescence and labelled ISV (intersegmental vessel), CA (caudal artery), DLAV (dorsal longitudinal anastomotic vessel) and CVP (caudal vein plexus) showed regular development in the WT and embryo injected with Control MO. In embryos injected with the ATG or Splice MO false connections between neighbouring ISVs were formed (indicated by white arrow heads), the DLAV was interrupted (indicated by asterisks) and the caudal vein plexus was irregular in appearance in both morphants. Co-injection of NOSTRIN mRNA with the Splice MO almost completely re-established the ISV trajectory, DLAV integrity and CVP regularity. (**D**) The efficient KD of NOSTRIN after injection of ATG MO or Splice MO and the expression of NOSTRIN after mRNA co-injection were verified by immunoblotting of whole fish lysates prepared at 48 hpf using a NOSTRIN-specific antiserum, an immunoblot of vinculin demonstrated loading of equal amounts. (**E**) Quantitative analysis of live embryos at 48 hpf treated as indicated; vascular phenotype included abnormal ISV trajectory, DLAV discontinuity, oedema, haemorrhaging.

tip cells (Figure 3E) and the number of filopodia at the leading edge of the expanding vascular plexus (Figure 3F and J) were reduced and the average length of tip cell filopodia was greatly diminished (Figure 3I and J). This indicates a function of NOSTRIN in the regulation of proliferation and migration as endothelial cell key characteristics and confirms the role of NOSTRIN in tip cell filopodia formation and sprouting angiogenesis *in vivo*.

In order to investigate whether the requirement for NOSTRIN is cell-autonomous or nonautonomous with regard to endothelial cells, we analysed key parameters of the retinal vasculature in NOSTRIN KO mice with Tie2-Cre-mediated

deletion of the NOSTRIN gene (NOSTRIN EC KO, Supplementary Figure S5). Spreading of the vascular plexus, the vascularised area, the number of branch points, the number of tip cells and the number of tip cell filopodia were significantly reduced in NOSTRIN EC KO mice (Supplementary Figure S6A–E). Moreover, we found that cell proliferation was decreased (Supplementary Figure S6F and G) and observed less long filopodial extensions on NOSTRIN EC KO tip cells (Supplementary Figure S6H and I). Therefore we conclude, that NOSTRIN acts cell-autonomously to facilitate endothelial cell proliferation and migration.

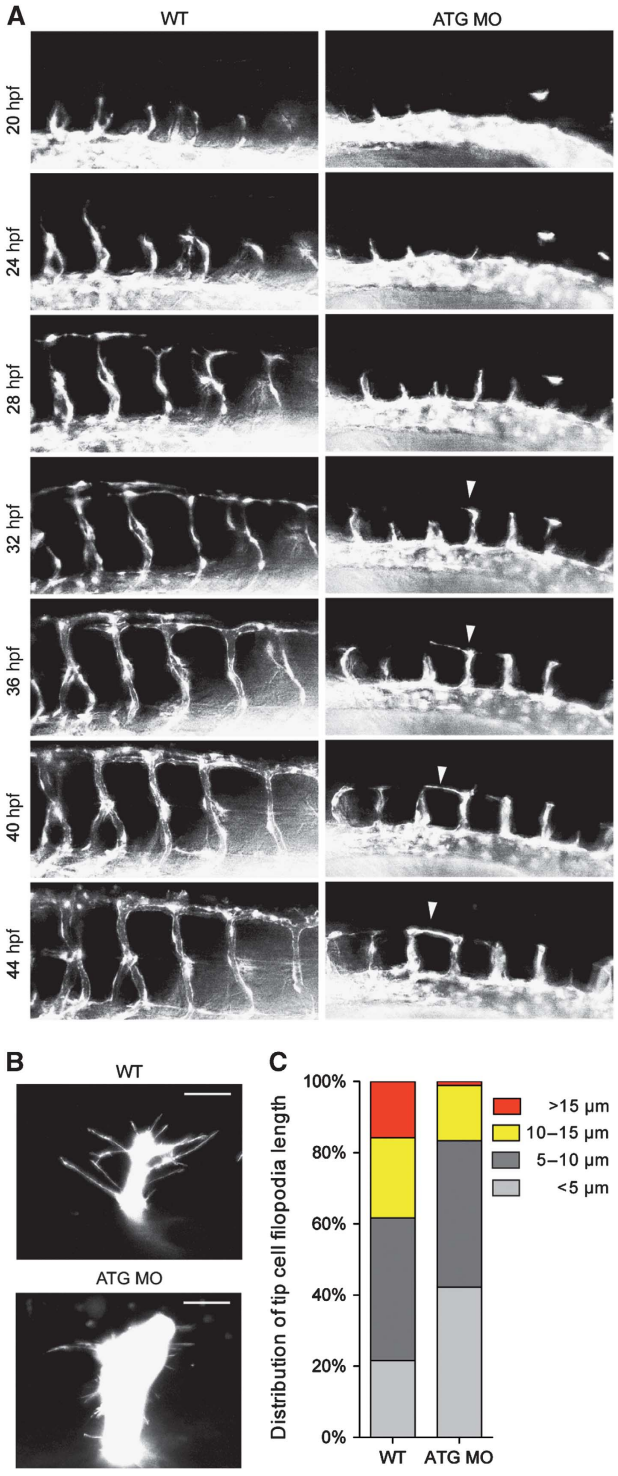

Figure 2 NOSTRIN morphants show an abnormal ISV trajectory phenotype associated with altered tip cell morphology and filopodia length. (**A**) Time-lapse microscopy of developing ISVs. Images are lateral views with the anterior to the left and the dorsal side up and were extracted from Supplementary Videos 1 (WT) and 2 (ATG MO). Images show developing ISVs and DLAVs in the trunk region of WT *Tg(fli1a:EGFP)*^{y1} embryos (left) in comparison to embryos injected with ATG MO (right) visualised by eGFP fluorescence and analysed at the indicated time points between 20 and 44 hpf. The white arrowhead indicates an ISV tip cell in the ATG MO-injected embryo, which did not migrate more dorsally than the level of the horizontal myoseptum after 32 hpf, but extended a prominent protrusion along the longitudinal body axis at approx. 36 hpf. It formed an irregular connection with the neighbouring ISV at the level of the horizontal myoseptum at approx. 42 hpf. (**B**) Reduced filopodia length of ISV tip cells. CLSM images of leading tip cells of ISV sprouts in the trunk region of WT *Tg(kdrl:eGFP)*^{s843} (top) and ATG-MO injected embryos (bottom) visualised by eGFP fluorescence and analysed at 24 hpf. The scale bar represents 15 µm. (**C**) Distribution of tip cell filopodia length. Analysis of filopodia length in ISV tip cells equivalent to those shown in (**B**) revealed a reduction in the percentage of long filopodia in the ATG MO-injected embryos in comparison to WT. For analysis of filopodia length images of 6–8 tip cells from 2 WT and 2 ATG MO injected embryos were used.

NOSTRIN interacts with and activates Rac1

Angiogenic behaviour of endothelial cells is critically controlled by the activity of small GTPases (Tan *et al*, 2008; De Smet *et al*, 2009; Epting *et al*, 2010; Wang *et al*, 2010). To understand the molecular basis for NOSTRIN function in this process, we analysed the interaction of NOSTRIN with the three prototypic Rho family GTPases, Cdc42, Rac1 and RhoA in a GST-pulldown assay. Since full size NOSTRIN is characterised by low solubility, for the following experiments we used soluble deletion mutants of NOSTRIN, which lack either the N-terminal F-BAR domain, NOSTRINΔFBAR (aa225–506), or the C-terminal SH3 domain, NOSTRINΔSH3 (aa1–440) (Figure 4A). NOSTRIN interacted strongly and specifically with the activated form of Rac1 (GST-Rac1-GTPγS) and to lesser extent with the activated form of Cdc42 (GST-Cdc42-GTPγS), while we detected no interaction with RhoA (Figure 4B). NOSTRIN did not interact significantly with the inactive GDP-bound forms of any of the GTPases (Figure 4B). In order to analyse whether the interaction of NOSTRIN with Rac1 and Cdc42 was direct, we performed a GST-pulldown assay using recombinantly expressed and purified proteins. In accordance with our previous results, NOSTRIN interacted directly and specifically with the active GTPγS-bound form of Rac1 and only weakly with inactive GDP-bound and nucleotide free Rac1. We could also confirm that NOSTRIN bound weakly to active GTPγS-bound Cdc42 (Figure 4C). We next tested whether the interaction of NOSTRIN with Rac1 depends on the presence of the HR1 motif (homology region 1, aa 304–386 in NOSTRIN; Figure 4A), which in other F-BAR proteins mediates the interaction with small GTPases of the Rho family (Ho *et al*, 2004; Heath and Insall, 2008; Frost *et al*, 2009; Roberts-Galbraith and Gould, 2010). We used mammalian cells expressing a construct with additional

deletion of the HR1 motif, NOSTRINΔFBAR/ΔHR1 (aa225–311 fused to 383–506) and found that the interaction was abolished, when the HR1 motif was deleted (Figure 4D), indicating that the interaction between NOSTRIN and Rac1 is indeed mediated by the HR1 motif.

To test if NOSTRIN is involved in Rac1 activation, we determined Rac1 activity by PAK-CRIB pulldown experiments and found that overexpression of full size NOSTRIN led to a pronounced activation of Rac1 in comparison to the expression of GFP in control cells (Figure 5A). To determine, if the HR1 motif was necessary for the NOSTRIN-dependent activation of Rac1, we compared Rac1 activity in cells that overexpressed NOSTRIN or the deletion mutant NOSTRINΔHR1 (aa1–311 fused to 383–506). Indeed, NOSTRINΔHR1, which is unable to bind to Rac1, did not induce Rac1 activation (Figure 5A). This suggested that the interaction of Rac1 with NOSTRIN via its HR1 motif is necessary for Rac1 activation.

NOSTRIN interacts with the Rac1 GEF Sos1 to activate Rac1

A possible explanation for this NOSTRIN-induced activation of Rac1 would be the recruitment of a guanine nucleotide exchange factor (GEF). Therefore we analysed the interaction of NOSTRIN with three previously described Rac1 GEFs, Sos1, Tiam1 and Vav2 (Michiels *et al*, 1995; Abe *et al*, 2000; Sini *et al*, 2004). We found that GST-NOSTRIN full size (aa1–506) interacted with endogenous Sos1 in the lysates of primary endothelial cells, while we could not detect an interaction between NOSTRIN and Tiam1 or Vav2 (Figure 5B). Since Sos1 is known to interact with SH3 domains via its proline-rich domain (Rozakis-Adcock *et al*, 1993), we analysed whether the SH3 domain of NOSTRIN was necessary for the NOSTRIN/Sos1 interaction in a series of experiments. For this purpose we used GST-NOSTRIN full size (aa1–506), GST-NOSTRINΔSH3 (aa1–440) and GST-NOSTRIN-SH3 (aa433–506), where the SH3 domain was fused to GST. Indeed, the interaction between NOSTRIN and Sos1 was abolished when the NOSTRIN SH3 domain was deleted (Figure 5B and C) and occurred also between the isolated SH3 domain of NOSTRIN and endogenous Sos1 (Figure 5C), indicating that the NOSTRIN SH3 domain is necessary and sufficient to mediate the interaction with Sos1. Finally, to experimentally prove that the NOSTRIN/Sos1 interaction was direct, we tested the interaction of the three GST-NOSTRIN fusion proteins with the purified recombinant His-tagged proline-rich domain of Sos1 (His-Sos1-PRD). Indeed, His-Sos1-PRD interacted with full size NOSTRIN and the isolated SH3 domain, but not with the SH3 deletion mutant, confirming our previous results (Figure 5D).

We hypothesised that the activation of Rac1 upon NOSTRIN overexpression might be due to the recruitment of the Rac1 GEF Sos1 via the NOSTRIN SH3 domain towards the NOSTRIN binding partner Rac1. If this is correct, a NOSTRIN mutant incapable of binding Sos1, should not be able to induce Rac1 activation. Indeed, overexpression of the deletion mutant lacking the SH3 domain, NOSTRINΔSH3, which is able to bind Rac1 (Figure 4C) but not Sos1 (Figure 5B and C), did not lead to Rac1 activation in the PAK-CRIB pulldown assay (Figure 5A). This is in accordance with the initial hypothesis that NOSTRIN recruits Sos1 to Rac1 and thereby facilitates its activation.

NOSTRIN is required for FGF-2-dependent activation of Rac1 in primary endothelial cells

As an F-BAR protein NOSTRIN might function as a multivalent adaptor to link Rac1 activation to an upstream stimulus. In order to search for such novel interacting proteins, that might induce the NOSTRIN-mediated activation of Rac1, we performed a yeast-two-hybrid (Y2H) screen using the C-terminal portion of human NOSTRIN (aa362–506) as bait. With this approach, we identified a 255 amino acid fragment of the cytoplasmic tail of FGFR1 (aa547–801) as a novel interacting protein of NOSTRIN (Figure 6A). We confirmed the interaction of endogenously expressed full size proteins in mammalian cells by co-immunoprecipitation of FGFR1 with NOSTRIN using a polyclonal NOSTRIN-specific antiserum (Figure 6B).

The NOSTRIN bait fragment used for Y2H contained the SH3 domain and a sequence we refer to as intermediate domain (ID), because it lies in between the HR1 and SH3 domain (Figures 4A and 6A). In order to determine through which domain NOSTRIN interacts with the FGFR1, we analysed the NOSTRIN ID and SH3 domain individually in the Y2H system. The bait protein consisting of the NOSTRIN ID (aa 362–434) only, was still able to interact with FGFR1, while interaction was abolished when the bait contained only the SH3 domain (aa 434–506)(Figure 6A). Accordingly, GST-NOSTRINΔSH3 interacted with endogenous FGFR1 in a GST-pulldown assay from mammalian cell lysate, while GST-NOSTRIN-SH3 failed to interact (Figure 6C). Finally, in a direct protein/protein interaction assay using purified proteins, GST-NOSTRIN and GST-NOSTRINΔSH3 interacted with a C-terminal fragment of FGFR1 (aa692–822), while GST-SH3 again did not interact (Figure 6D). Taken together, this indicated that NOSTRIN and the FGFR1 interact in mammalian cells and suggests that the interaction is direct and dependent on the NOSTRIN ID and the C-terminal tail of the FGFR1.

In light of the ability of NOSTRIN to interact with FGFR1 on the one hand and to promote the activity of Rac1 on the other, the arising question was whether NOSTRIN was involved in the FGF-2-dependent activation of Rac1 in endothelial cells. To study this, we isolated primary mouse lung endothelial cells (MLECs) from WT and NOSTRIN KO mice by immunoselection and confirmed the expression of NOSTRIN in WT MLECs and its absence in KO cells by immunoblotting (Figure 7A). Interaction of NOSTRIN with the FGFR1 in endothelial cells was verified by co-immunoprecipitation. NOSTRIN and FGFR1 interacted strongly after stimulation with FGF-2, while no interaction was detectable in starved cells (Figure 7B), indicating that NOSTRIN interacted with FGFR1 in a stimulus-dependent fashion in endothelial cells. FGF-2 caused a significant activation of Rac1 in lysates of NOSTRIN WT MLECs. In contrast, FGF-2 was unable to activate Rac1 in NOSTRIN KO cells (Figure 7C). In order to analyse, if the action of NOSTRIN is specific for the FGFR1 or might also be directed towards other pro-angiogenic growth factors, we stimulated MLECs from NOSTRIN WT and KO mice with VEGF and found that VEGF induced Rac1 activity also when NOSTRIN was absent (Supplementary Figure S7). Taken together, this confirms our findings that NOSTRIN is favourable for the activation of Rac1 and demonstrates that FGF-2-dependent activation of Rac1 in primary endothelial cells depends on NOSTRIN.

NOSTRIN is necessary for FGF-2-dependent angiogenic response in the matrigel plug assay

Finally, we analysed the angiogenic response of WT and NOSTRIN KO mice to FGF-2 in the matrigel plug assay. For this purpose, adult male mice received two matrigel implants each, one containing vehicle and the other supplemented with FGF-2 to induce microvessel growth into the plug. After 10 days the implants were removed, processed for immunohistochemistry and the angiogenic response was measured as the area covered by PECAM-stained cells. We observed that

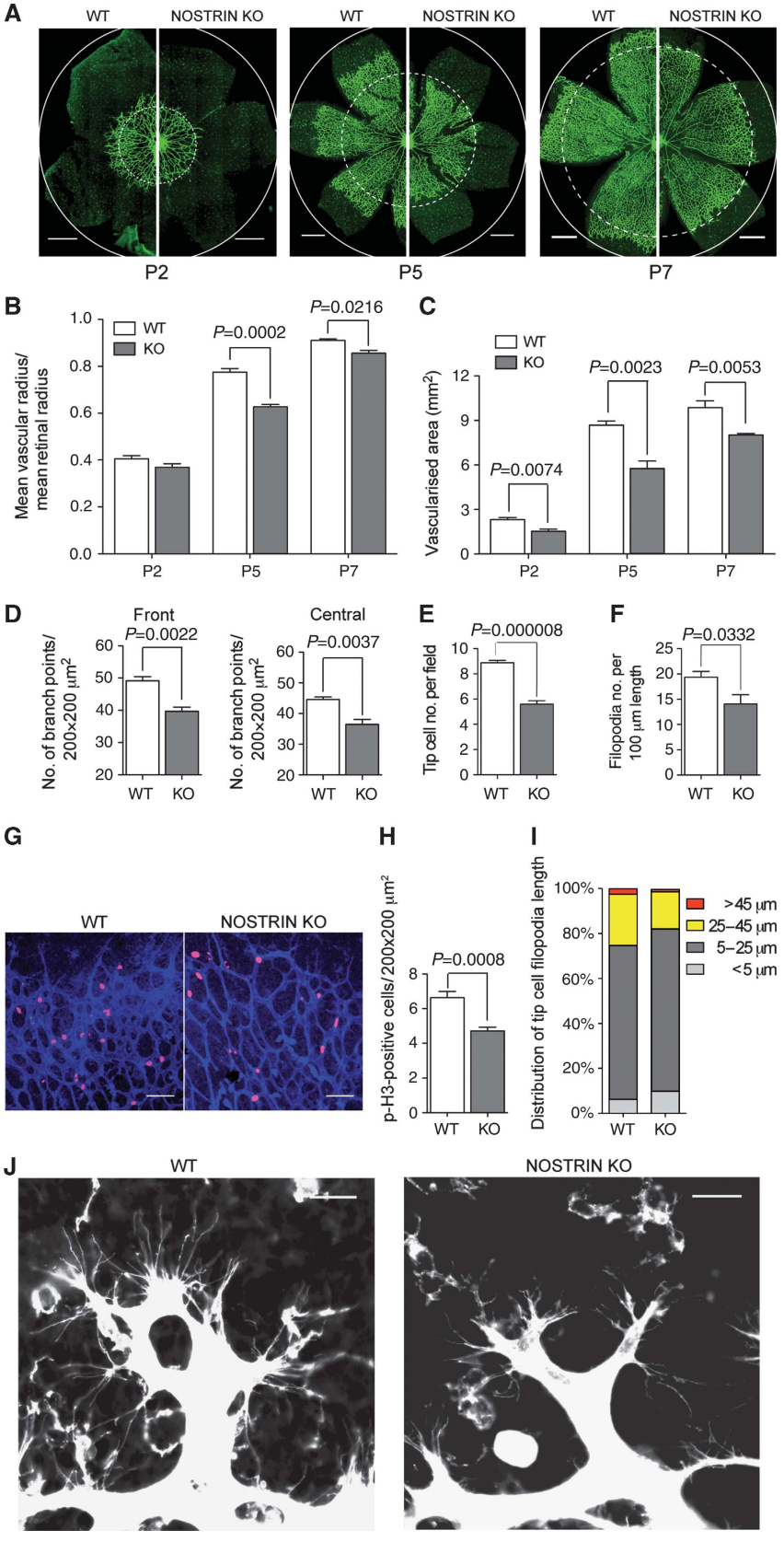

FGF-2 induced neovascularisation of matrigel implants in WT controls, whereas the angiogenic response was impaired in NOSTRIN KO mice (Figure 7D and E for quantification). In addition, in the absence of FGF-2, single, scattered PECAM-positive cells had entered the matrigel plug in WT mice and this was also reduced in the NOSTRIN KO (Figure 7D and E for quantification). NOSTRIN is thus required for proper postnatal FGF-2-induced angiogenesis *in vivo*.

Discussion

In this study we show that the F-BAR protein NOSTRIN is a novel, important factor for vascular morphogenesis. The loss of NOSTRIN causes defects in developmental angiogenesis characterised by changes in tip cell number and morphology, with a reduction of tip cell filopodia abundance and length and a decrease in endothelial cell proliferation. This is associated with the loss of the proper ISV trajectory in zebrafish and the impairment of spreading and branching of the vascular plexus of the postnatal retina in mice.

NOSTRIN KO mice are viable and we did not observe equally strong defects in vascular development during embryogenesis in mice as in zebrafish and it remains to be determined if other F-BAR proteins might at least partially compensate for the loss of NOSTRIN in the KO mouse. Phenotypic divergence between mice and zebrafish in terms of vascular development, however, is not unusual and occurs in a similar form e.g. upon the loss of NOGO A/B (Acevedo *et al*, 2004; Zhao *et al*, 2010).

During developmental angiogenesis NOSTRIN serves as a multivalent adaptor for FGFR1, Rac1 and its GEF Sos1 and the assembly of this signalling complex is necessary for the FGF-2-dependent activation of Rac1 (Figure 7F). In the context of this current study, the function of NOSTRIN is distinct from the previously reported role of NOSTRIN in the regulation of eNOS localisation and function. This is supported by the facts that 1) eNOS-derived NO is dispensable for postnatal retinal angiogenesis, which is normal in eNOS KO mice (Al-Shabrawey *et al*, 2003), and 2) there is no genetic evidence for the existence of an eNOS gene in zebrafish, although immunoreactivity with a eNOS-specific antibody has been reported (North *et al*, 2009).

We identify NOSTRIN as a novel binding partner of FGFR1, a well-known receptor for pro-angiogenic signals in endothelial cells (Presta *et al*, 2005; Horowitz and Simons, 2008; De Smet *et al*, 2009). FGF-2 or FGFR1, respectively, have been shown to promote proliferation and migration of endothelial cells and increase vascular density and branching in various *in vitro*, *ex vivo* and *in vivo* models (Feraud *et al*, 2001; Sheikh *et al*, 2001; Tomanek *et al*, 2001, 2010; Javerzat *et al*, 2002; Akimoto and Hammerman, 2003; Rousseau *et al*, 2003; Magnusson *et al*, 2004, 2005, 2007; Nicoli *et al*, 2009; Woad *et al*, 2012). However, the analysis of FGFR1 function in developmental angiogenesis has been complicated by the early lethality of FGFR1 knockout mice before the onset of vascularisation (Deng *et al*, 1994). The defects in proliferation, migration and branching we have observed upon KD of NOSTRIN in developing zebrafish and in NOSTRIN KO mice are in accordance with the known functions of FGF-2/FGFR1 in angiogenesis.

The association of NOSTRIN with FGFR1 is direct as suggested by the Y2H interaction and verified by interaction analysis with recombinantly expressed and purified proteins. The interaction occurred in cells cultured in the presence of serum, and upon stimulation with FGF-2, but not in starved cells, suggesting that the interaction might be regulated in an FGF-2-dependent manner. NOSTRIN interacts with the C-terminal tail of the FGFR1 (aa692–822). Interestingly, the C-terminal domain of FGFR1 (aa759–822) has been identified as crucial for mediating chemotaxis in endothelial cells (Landgren *et al*, 1998). This is in agreement with our model, which predicts that disassembly of the FGFR1/NOSTRIN/Rac1/Sos1 signalling complex either by the loss of NOSTRIN or truncation of the receptor would interfere with directed migration of endothelial cells.

Several members of the F-BAR protein family have been implicated in the trafficking of trans-membrane receptors such as the EGF- and the PDGF-receptor. However, no direct interaction of the receptor and the F-BAR protein has been reported in either case (Hu *et al*, 2009; Toguchi *et al*, 2010). We have shown previously that NOSTRIN facilitates the internalisation of eNOS through its binding to dynamin and N-WASP (Icking *et al*, 2005), therefore it is conceivable that NOSTRIN might also influence FGFR1 endocytosis. In respect to the specificity of NOSTRIN towards FGFR1, we so far do not have indications that NOSTRIN might bind to other trans-membrane receptors. In our Y2H interaction screen we did not find other growth factor receptors to interact with NOSTRIN and the VEGF-dependent activation of Rac1 in endothelial cells was unaffected when NOSTRIN was

Figure 3 Postnatal retinal angiogenesis is impaired in NOSTRIN knockout mice. (**A**) Side-by-side comparison of the retinal vasculature of NOSTRIN wild type (WT) and knockout (KO) mice. Retina flat mounts of postnatal days (P)2, P5 and P7, vasculature visualised by isolectin B4-FITC staining and analysed by CLSM. Dashed circles denote the vascular front in the KO, circles indicate the retinal margin in both genotypes. Scale bars represent 500 μm. (**B**) Quantification of retinal vasculature spreading. The mean vascular radius (distance between vascular front and centre of the optic disc) of 4–6 retinas for each genotype and time point was calculated and expressed relative to the mean retinal radius. (**C**) Comparison of vascularised area. The vascularised area of 4–6 retinas for each genotype and time point was determined using AxioVision software (Rel 4.8.2 Zeiss). (**D**) Comparison of number of branch points. Branch points were counted in 5–8 fields in the front (peripheral to two-thirds of the vascular radius) and the central part of the vascularised area (between one-third and two-thirds of the vascular radius), 4 retinas for each genotype at P5. (**E**) Quantification of tip cell number. Tip cells (defined as blind-end endothelial protrusions with associated filopodial bursts at the angiogenic front) were counted in 15 fields per retina, 5–6 retinas for each genotype. (**F**) Quantification of filopodia number. Filopodia of tip cells at the vascular front were counted in 15 fields per retina, 5–6 retinas for each genotype and expressed as filopodia number per 100 μm vessel length. (**G**) Vascular front of retina flat mounts at P5 with mitotic nuclei stained using a phospho-Histone H3 (p-H3)-specific antibody in combination with isolectin B4-FITC as described above. Scale bars represent 70 μm. (**H**) Quantification of p-H3-positive endothelial cells. p-H3-positive cells were counted in 8 fields per retina (vascular front) and 6 retinas per genotype. (**I**) Distribution of tip cell filopodia length. Measurement of filopodia length was done on 6 fields per retina, 5 retinas for each genotype. (**J**) Comparison of retinal tip cells at the vascular front. Representative high magnification CLSM images of the vascular front of P5 retina flat mounts as depicted in (**A**) show that tip cells in the KO have less and shorter filopodial protrusions than tip cells in WT retinas. Scale bars represent 20 μm. Data shown in (**B**), (**C**), (**D**), (**E**), (**F**) and (**H**) are means ± s.e.m. Data were analysed by unpaired two-tailed *t*-test and *P*-values are shown.

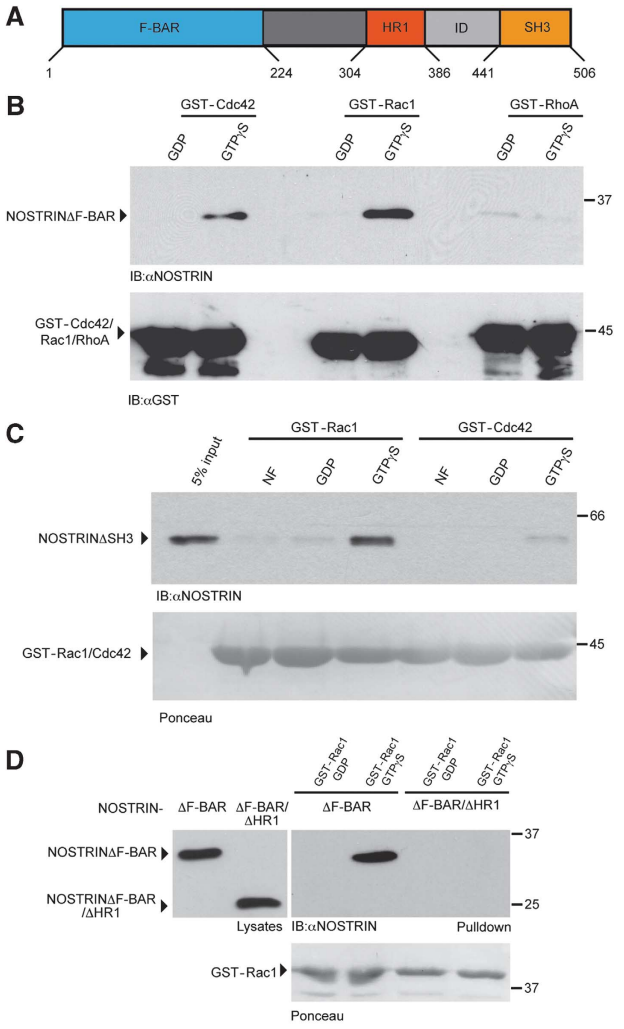

Figure 4 NOSTRIN interacts with Rac1 via the HR1 motif. (**A**) Domain structure of NOSTRIN. Amino acid numbers indicate the N- and C-terminal borders of the F-BAR, HR1, ID (intermediate domain) and SH3 domains. (**B**) NOSTRIN interacts with Rac1. GDP- or GTPγS-loaded GST-Cdc42, GST-Rac1 and GST-RhoA were used for GST-pulldown experiments using cell lysates expressing NOSTRIN. NOSTRIN (NOSTRINΔF-BAR) interacted specifically with GTPγS-loaded GST-Rac1 and to a lesser extent with GTPγS-loaded GST-Cdc42, while it did not interact with RhoA, independent of the nucleotide bound. (**C**) NOSTRIN interacts directly with active Rac1. Nucleotide free (NF), GDP- or GTPγS-loaded GST-Rac1 or GST-Cdc42 were used for GST-pulldown experiments in combination with purified recombinant NOSTRINΔSH3. 5% of the amount of purified NOSTRINΔSH3 used for GST-pulldown is shown for comparison of protein levels (5% input). NOSTRIN (NOSTRINΔSH3) interacted strongly and directly with GTPγS-loaded GST-Rac1. (**D**) NOSTRIN interacts with Rac1 via the HR1 motif. GDP- or GTPγS-loaded GST-Rac1 was used for GST-pulldown experiments using cell lysates expressing NOSTRINΔF-BAR and NOSTRINΔF-BAR/ΔHR1. Immunoblot from cell lysates shows expression of equal amounts of NOSTRINΔF-BAR and NOSTRINΔF-BAR/ΔHR1 (left). In the GST-Rac1 pulldown GTPγS-loaded GST-Rac1 interacted specifically with NOSTRINΔF-BAR, but not with NOSTRINΔF-BAR/ΔHR1 (right). (**B–D**) NOSTRIN was detected by immunoblotting with NOSTRIN-specific antibody (Mookerjee *et al*, 2007). Equal amounts of GST-Rac1, GST-Cdc42 or GST-RhoA, respectively, were used, detected by immunoblotting with a GST-specific antibody or Ponceau staining, as indicated.

absent, indicating that NOSTRIN does not bind to a broad variety of receptors or unspecifically modulates signal transduction.

In addition to the direct interaction with FGFR1, in this study we have identified the small GTPase Rac1 and its GEF Sos1 as novel direct binding partners of NOSTRIN. The interaction of NOSTRIN with Rac1 is mediated by the HR1 motif, an interaction motif shared between several F-BAR proteins (Heath and Insall, 2008; Frost *et al*, 2009). The interaction with Sos1 involves NOSTRIN's SH3 domain and the PRD of Sos1. Moreover NOSTRIN induces Rac1 activation dependent on both the HR1 and the SH3 domain, suggesting that NOSTRIN might serve as an adaptor to facilitate the interaction of Rac1 and its GEF in order to promote Rac1 activation. NOSTRIN preferentially interacts with active Rac1 and this would be consistent with the idea that NOSTRIN participates in an activation loop, amplifying Rac1 activation. Endothelial Rac1 is important for cell migration and vascular development in mice (Tan *et al*, 2008; D'Amico *et al*, 2009) and for developmental angiogenesis in zebrafish (De Smet *et al*, 2009; Epting *et al*, 2010; Wang *et al*, 2010), however, the precise role of Rac1 in endothelial tip cell function is not fully understood. Correct spatial positioning and activation of Rac1 are important for the highly polarised character of endothelial cells (Tzima, 2006; De Smet *et al*, 2009) and it might be possible that NOSTRIN serves to coordinate FGFR1 stimulation with spatial activation of Rac1. The dual effect of FGF2/FGFR1 on directed migration and proliferation is also observed in the case of VEGF-A/VEGFR2, where the VEGF-A gradient serves as tip cell guidance cue and the VEGF-A concentration regulates proliferation in stalk cells (Gerhardt *et al*, 2003). Therefore the NOSTRIN/Rac1/Sos1 signalling complex might serve to detect the FGF-2 signal both in tip and stalk cells; while it is translated into directional migration in tip cells, it stimulates proliferation in stalk cells. However, we cannot rule out that other FGFR1-dependent signal cascades might be involved e.g. MAP kinase signalling.

The pro-angiogenic effect of FGF-2 is diminished *in vivo* in the matrigel plug assay, if NOSTRIN is absent. In accordance with our findings, it has been shown that the FGF-2-induced angiogenesis into matrigel plugs depends on Rac1 (Dormond *et al*, 2001), highlighting the importance of Rac1 to mediate the angiogenic effect of FGF-2. In addition, we have employed the zebrafish yolk sac angiogenesis assay (Nicoli *et al*, 2009) to test for FGF-2 induced angiogenesis from the SIV basket *in vivo*. However, the impaired SIV development in NOSTRIN morphants prevented a conclusive interpretation. Taken together, our data strongly suggest that NOSTRIN is indeed involved in FGFR1-dependent signal transduction *in vitro* and *in vivo*. Our model is different from the previously proposed mechanism, where FGF-2 has been shown to activate Rac1 independently of FGFR1 through the low affinity heparan sulphate proteoglycan syndecan-4, involving the action of the RhoG/ELMO1/Dock180 GEF complex (Elfenbein *et al*, 2009). A potential crosstalk between the different pathways controlling the spatial activation of Rac1 remains to be determined.

F-BAR proteins are typically involved in the generation of positive membrane curvature and plasma membrane invaginations, e.g. during endocytosis (Heath and Insall, 2008; Frost *et al*, 2009; Qualmann *et al*, 2011). In contrast, I-BAR (inverse BAR) proteins generate negative membrane curvature and induce plasma membrane protrusions, such as lamellipodia and filopodia (Ahmed *et al*, 2010; Zhao *et al*,

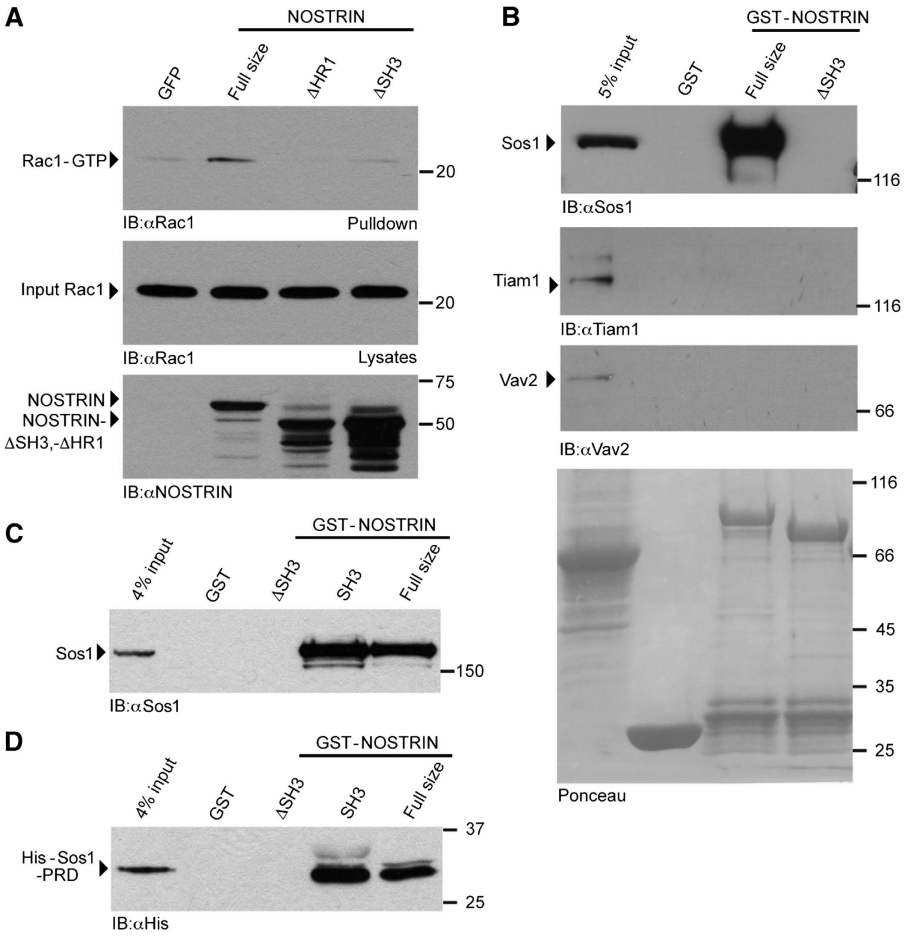

Figure 5 NOSTRIN interacts with the Rac1 GEF Sos1 and induces Rac1 activation. (**A**) NOSTRIN overexpression induces Rac1 activation depending on the presence of the HR1 and the SH3 motif. NOSTRIN, NOSTRINΔHR1, NOSTRINΔSH3 or GFP were expressed using the SFV-system and the activity of Rac1 measured as amount of Rac1-GTP precipitated with the CRIB domain of PAK (PAK-CRIB assay). Equal amounts of Rac1 (input Rac1) and NOSTRIN, NOSTRINΔHR1 and NOSTRINΔSH3 were applied. Overexpression of NOSTRIN induced strong Rac1 activation in comparison to GFP, the deletion mutants NOSTRINΔSH3 and NOSTRINΔHR1 did not induce Rac1 activation. (**B**) NOSTRIN interacts with Sos1. GST-pulldown from primary mouse lung endothelial cells using GST-NOSTRIN, GST-NOSTRINΔSH3 or GST alone indicated specific interaction of full size NOSTRIN with endogenous Sos1, but not with Tiam1 or Vav2. Deletion of the SH3 domain in NOSTRINΔSH3 resulted in loss of the NOSTRIN/Sos1 interaction. (**C**) NOSTRIN SH3 domain is sufficient for interaction with Sos1. GST-pulldown from cell lysate using GST-NOSTRIN, GST-NOSTRINΔSH3, GST-SH3 or GST alone indicated specific interaction of endogenous Sos1 with GST-NOSTRIN and the isolated SH3 domain GST-SH3. (**D**) NOSTRIN SH3 domain binds the proline-rich domain of Sos1. GST-pulldown with recombinantly expressed and purified proline-rich domain of Sos1 (His-Sos1-PRD) confirmed specific and direct interaction of Sos1 with GST-NOSTRIN and GST-SH3.

2011). In this study we have observed, that the loss of NOSTRIN affects filopodia formation, but we did not analyse if this is a direct effect of loss of the F-BAR domain or a consequence of altered Rac1 activity or cytoskeletal processes. Both scenarios seem possible, since—deviating from the classification described above—the F-BAR domain of srGAP2 (Slit/Robo Rho GTPase activating protein-2) generates negative membrane curvature and promotes the formation of plasma membrane protrusions, suggesting that F-BAR proteins can have a more versatile function in membrane dynamics (Guerrier *et al*, 2009; Zhao *et al*, 2011).

With this study we demonstrate that NOSTRIN is necessary for proliferation, directed migration and filopodia formation in endothelial cells. NOSTRIN is the first F-BAR protein for which a function in developmental angiogenesis is demonstrated and illustrates an evolving common theme in F-BAR protein biology (Hu *et al*, 2009; Koduru *et al*, 2010; Toguchi *et al*, 2010): in addition to co-ordinating events involving the plasma membrane and the cytoskeleton, such as endocytosis, F-BAR proteins serve to integrate extracellular signals and are essential for complex biological processes such as neuronal guidance and vascular development.

Materials and methods

Zebrafish MO injection and analysis

Control MO CCTCTTACCTCAGTTACAATTTATAT, translation blocking ATG MO GCTGCTCAGCGGGTCCTTCATCTTC and splice blocking MO TCCAACACGTCTCCTGGCAGATC were diluted in ultrapure water with 0.05% phenol red. 3.3 ng of Control MO, 3.3 ng of ATG MO or 5 ng of Splice MO were injected into 2–8 cell stage *Tg(fli1a:EGFP)*^{y1} (Lawson and Weinstein, 2002) or *Tg(kdrl:EGFP)*^{s843} (Jin *et al*, 2005) zebrafish embryos. For rescue experiments full size zebrafish NOSTRIN cDNA clone: IRBOp991F08104D (NCBI Reference Sequence: NM_001039724.3) was purchased from *Imagenes* and cloned into the vector pcDNA3.1 (Invitrogen). mRNA was prepared using the mMessage mMachine kit (Ambion) and 15 pg co-injected with the Splice MO if not stated otherwise.

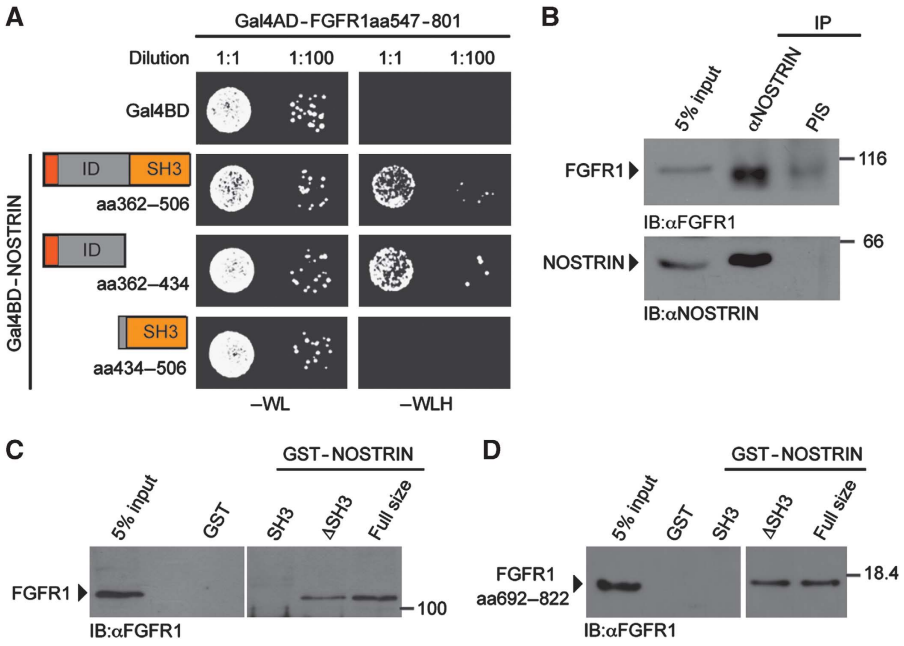

Figure 6 NOSTRIN interacts with FGFR1 (**A**) Y2H interaction analysis between FGFR1 and NOSTRIN. Co-expression of a fusion protein of the Gal4 activator domain (Gal4AD) with the cytoplasmic tail of the FGFR1 (Gal4AD-FGFR1aa547–801) with 3 separate fusion proteins between the Gal4 DNA binding domain (Gal4BD) with distinct C-terminal NOSTRIN fragments (Gal4BD-NOSTRINaa362–506, Gal4BD-NOSTRINaa362–434 and Gal4BD-NOSTRINaa434–506). Gal4BD co-transformed with Gal4AD-FGFR1aa547–801 served as control. Each co-transformed yeast clone was spotted onto growth medium devoid of tryptophan and leucin (− WL) and growth medium devoid of tryptophan, leucine and histidine (− WLH) in 2 different dilutions. Growth of co-transformed yeast colonies on − WL indicates lack of toxicity, growth on − WLH of yeast co-transformants with Gal4AD-FGFR1aa547–801 in combination with either Gal4BD-NOSTRINaa362–506 or Gal4BD-NOSTRINaa362–434 indicates interaction, while no growth of yeast co-transformants with Gal4AD-FGFR1aa547–801 in combination with Gal4BD-NOSTRINaa434–506 indicates a lack of interaction. (**B**) NOSTRIN interacts with FGFR1 in mammalian cells. Co-immunoprecipitation of endogenous FGFR1 with endogenous NOSTRIN from cell lysates using a polyclonal NOSTRIN-specific antiserum for immunoprecipitation (IP). Lack of co-immunoprecipitation with pre-immune serum (PIS) served as specificity control. 5% of the volume of the cell lysate used for IP is shown for comparison of protein levels (5% input). Proteins are detected by immunoblotting with FGFR1-specific antiserum and a NOSTRIN-specific antibody (Mookerjee *et al*, 2007). (**C**) NOSTRIN interacts with FGFR1 independently of the SH3 domain. GST-pulldown experiment using GST-NOSTRIN, GST-NOSTRINΔSH3, GST-SH3 or GST alone to pulldown endogenous FGFR1 from cell lysates. Lack of interaction with GST indicates specificity. Proteins are detected by immunobloting with polyclonal FGFR1-specific antiserum. (**D**) Direct protein/protein interaction analysis. Recombinantly expressed and purified GST-NOSTRIN full size, GST-NOSTRINΔSH3, GST-SH3 or GST used in combination with a recombinantly expressed and purified C-terminal fragment of FGFR1 comprising aa 692–822, confirming interaction of FGFR1 with GST-NOSTRIN and GST-NOSTRINΔSH3 (FGFR1 aa692–822 was chosen because it could be purified as a soluble protein in sufficient amounts). Proteins were detected by immunoblotting with an FGFR1-specific antibody.

After all injections embryos were kept at 28°C in E3 medium (5 mM NaCl, 0.17 mM KCl, 0.33 mM $CaCl_2$, 0.33 mM $MgSO_4$). At indicated time points embryos were dechorionated, anaesthesized with tricaine (Sigma) and mounted in 1.2% low-melting-point agarose (Roth) in E3 medium. Bright field images were acquired using a Leica MZ165 dissecting microscope (Figure 1A–C). Fluorescent images were acquired using a Leica TCS SP5 confocal microscope (Figure 1D). Time-lapse microscopy images were captured every 10 min for 24 h with Leica Live Cell Imaging microscope (Figure 2A, Supplementary Videos 1 and 2). Length of tip cell filopodia was determined from high resolution images captured with Zeiss LSM510 confocal microscope using ImageJ software (Figure 2B). Zebrafish protein lysates were prepared in lysis buffer (1% NP-40, 150 mM NaCl, 2 mM EDTA, 50 mM Tris pH 7.4, protease inhibitor cocktail (*Roche*)) and analysed by immunoblotting.

Generation of NOSTRIN knockout mouse

NOSTRIN targeting vector construction and knockout mouse generation were carried out by genOway (www.genoway.com; Lyon, France). The targeting vector contained two loxP sites, one in the long homology region (6.0 kb, homologous to a sequence containing exons 3, 4 and 5) and a second one in the short homology region (2.0 kb, homologous to exon 6) of the *NOSTRIN* gene (GenBank accession number NM_181547), and a neomycin resistance gene cassette for positive selection flanked by *Frt* sites. Homologous recombination after introduction of the linearised vector in 129sv/Pas embryonic stem cells and neomycin selection resulted in generation of ES cell clones with a recombined *NOSTRIN* locus containing one loxP site between exon 3 and 4 and the *Frt*-flanked neomycin resistance gene cassette followed by the second loxP-site between exons 5 and 6. ES cell clones containing the recombined *NOSTRIN* allele were used for injection into C57BL/6J blastocysts and generation of chimera. Male offspring of chimera with recombined *NOSTRIN* allele was further mated with C57BL/6J Cre deleter females to induce excision of the floxed sequence (exons 4 and 5) to generate the *NOSTRIN* knockout allele. The presence of the *NOSTRIN* knockout allele in the offspring was confirmed by Southern blotting and PCR. Heterozygeous *NOSTRIN* knockout mice were backcrossed into C57BL/6J mice for 6 generations.

Analysis of mouse postnatal retinal angiogenesis

For flat mount retina staining, the intact eye was fixed in 4% paraformaldehyde (PFA). The retina was dissected, rinsed with PBS, and permeabilized in blocking buffer (1% BSA and 0.5% Triton-X-100 in PBS). After three washes with Pblec buffer (0.5% Triton-X-100, 1 mM $CaCl_2$, 1 mM $MgCl_2$, 0.1 mM $MnCl_2$ in PBS, pH 6.8), the retina was incubated in Pblec containing FITC-conjugated isolectin B4 (1:100, Sigma). For proliferation analysis additional staining with a phospho-Histone H3-specific antibody (anti-p-H3-Ser-10 mitosis marker, 1:100, MerckMillipore) in combination with an Alexa546-conjugated anti-rabbit antibody (1:200, Invitrogen) was carried out. Stained retinas were flat mounted and viewed with a Zeiss LSM 510 META confocal microscope. High-resolution CLSM Images were analysed using Axiovision software.

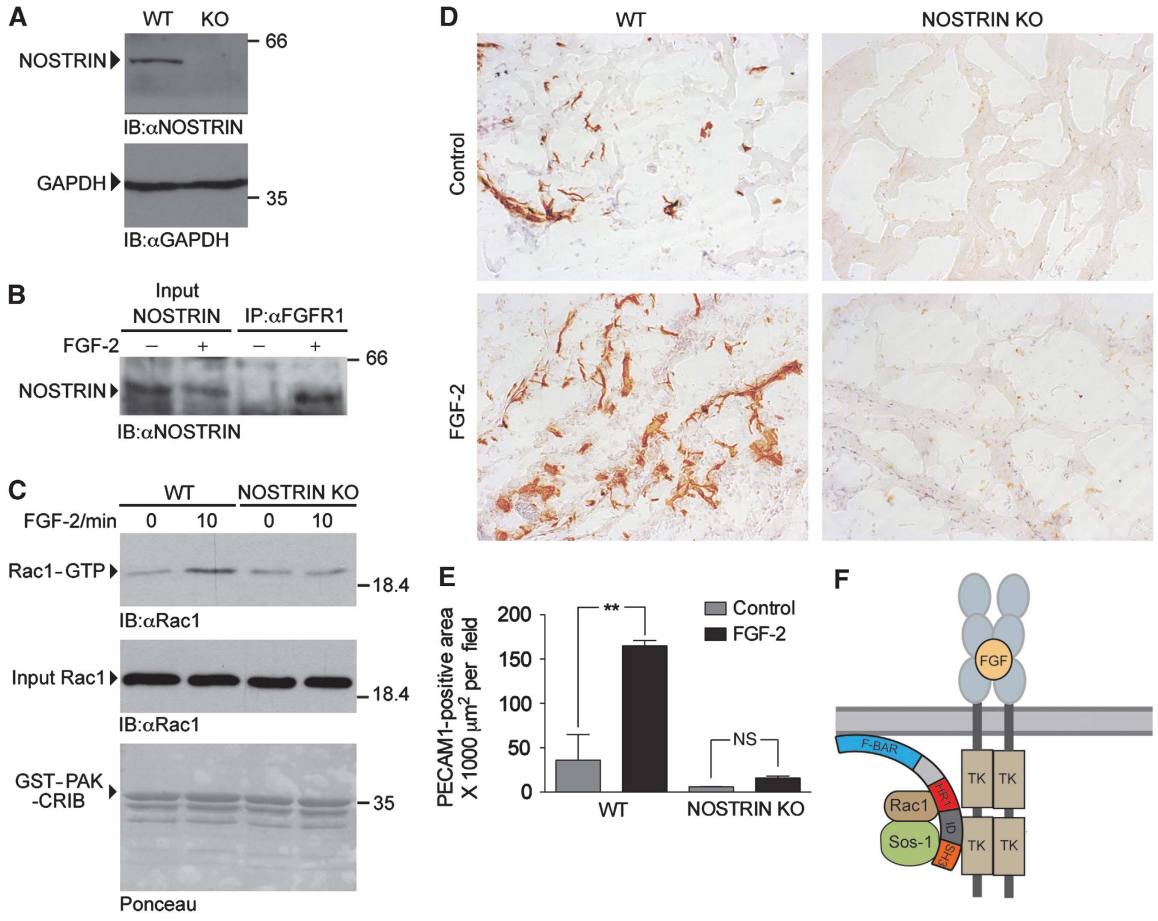

Figure 7 NOSTRIN is required for the FGF-2-dependent activation of Rac1 in primary endothelial cells and for the angiogenic response to FGF-2 in the matrigel plug assay. (**A**) NOSTRIN expression in mouse lung endothelial cells (MLECs). Confirmation by immunoblotting with a NOSTRIN-specific antiserum of the expression of NOSTRIN in MLECs isolated from WT mice and its absence in MLECs isolated from NOSTRIN KO mice; an immunoblot of GAPDH is shown as loading control. (**B**) NOSTRIN interacts with FGFR1 in MLECs. Specific co-immunoprecipitation of NOSTRIN with FGFR1 from lysates prepared from MLECs pretreated with FGF-2 (25 ng/ml, 5 min) or vehicle. An FGFR1-specific antibody was used for precipitation. NOSTRIN was detected by immunoblotting with a NOSTRIN-specific antiserum. (**C**) Comparison of FGF-2-dependent activation of Rac1 in MLECs isolated from WT or NOSTRIN KO mice. PAK-CRIB assays performed using equal amounts of Rac1 (input Rac1) and GST-PAK-CRIB. FGF treatment (25 ng/ml) induced Rac1 activity in WT, but not in KO MLECs. (**D**) Comparison of representative PECAM-stained cryosections of matrigel plugs implanted in WT and NOSTRIN KO mice in the absence (control) or the presence of FGF-2. FGF-2 (150 ng/ml) induced a strong angiogenic response after 10 d in WT, but not in NOSTRIN KO mice. (**E**) Quantification of PECAM-stained area and statistical analysis of 10 sections per matrigel plug, from 3 matrigel plugs per treatment and genotype. Data shown are means ± s.e.m. analysed by two-way ANOVA with Bonferonni post-test; $P<0.01$. (**F**) Model of the FGFR1/NOSTRIN/Rac1/Sos1 complex, discussed in the main text (TK – tyrosine kinase domain).

Matrigel plug assay

Growth factor reduced matrigel (BD Bioscience) was thawn overnight at 4°C and supplemented with 0.0025 U/ml heparin. Optional, 150 ng/ml FGF-2 was added to the matrigel. Eight week old male WT and NOSTRIN KO mice were anaesthetized by subcutaneous injection of 4% chloralhydrate solution (three animals per genotype). 500 μl matrigel supplemented with 150 ng/ml FGF-2 were injected subcutaneously, dorsolaterally on the right side of the animal and as a negative control matrigel without growth factor was injected on the left side. After ten days mice were sacrifised and matrigel plugs dissected from the tissue, embedded in Tissue-Tek (Sakura) and frozen at − 80°C. Frozen matrigel plugs were cut on a microtome at 16 μm slice thickness. Sections were fixed in acetone and stained with PECAM-1 antibody in combination with secondary biotin goat anti-rat antibody, Streptavidin-Horseradish Peroxidase Pre-dilute (BD Pharmingen) and DAB substrate kit (BD Pharmingen). Sections were counterstained with Mayer's hematoxylin solution. Images (10 per matrigel plug) were acquired using a Leica MZ165 dissecting microscope and PECAM-1 staining positive area determined with Adobe Photoshop CS4 software.

Isolation of mouse lung endothelial cells

Isolation of MLECs was carried out as described (Sawamiphak *et al*, 2010). In summary, lungs from 3–6 P4-P7 old pups were minced and digested with collagenase. Endothelial cells were sorted using rat anti-mouse PECAM-1 antibody (BD Pharmingen) coupled to anti-rat IgG coupled magnetic beads (Invitrogen). Cells were used for analysis in passage 2 and 3.

Yeast two hybrid (Y2H) screening

Y2H screening was performed according to the Yeast Protocol Handbook (Clontech). In brief, NOSTRINaa362–506 was cloned into pGBKT7 vector (coding for the DNA binding domain of Gal4, Gal4BD) and used as bait. Human kidney cDNA library in pACT2 vector (coding for the activator domain of Gal4, Gal4AD) was co-transformed together with the bait into yeast strain AH109 and growth on synthetic drop-out media (-W/-L/-H) was assessed to select for NOSTRIN interaction partners. Among others one clone was identified as aa547–801 of fibroblast growth factor receptor 1. For 'one-on-one' Y2H analysis NOSTRIN deletion mutants were cloned into pBD vector and cotransformed with pACT2-FGFR1aa547–801 into yeast (Figure 6A). Selection was done as above.

Purification of GST- and His-tag fusion proteins

GST-fusion proteins of Rac1, the CRIB domain of PAK (PAK-CRIB), C-terminal part of FGFR1, NOSTRIN and NOSTRIN deletion constructs were purified on glutathione (GSH)-Sepharose (GE Healthcare) as previously described (Icking *et al*, 2006). For the small GTPases and PAK-CRIB, lysis and wash buffer contained 5 mM $MgCl_2$. $(His)_6$-tagged fusion proteins of the Sos1 proline rich region (His-Sos-PRD) were purified from *E. coli* BL21 as previously described for $(His)_6$-tagged NOSTRIN (Icking *et al*, 2006).

SFV-mediated NOSTRIN expression and Rho GTPase interaction assay

Infection of CHO cells with Semliki Forest Virus was performed as described before (Zimmermann *et al*, 2002). Cells expressing SFV-NOSTRIN-ΔF-BAR or SFV-NOSTRIN-ΔF-BAR/ΔHR1 were lysed in GTPase lysis buffer (50 mM Tris–HCl pH 7.4, 150 mM NaCl, 5 mM $MgCl_2$, 0.5% Triton-X-100, 10 μM Aprotinin, 1 mM Benzamidin, 1mM PMSF). GDP or GTPγS (Sigma) was added to the cell lysates (final concentration 0.1 mM). GST-Rac1 coupled to GSH sepharose was loaded with either GDP or GTPγS in GTPase loading buffer (20 mM Tris–HCl pH 7.4, 25 mM NaCl, 5 mM EDTA, 2 mM of GDP or GTPγS), finally $MgCl_2$ was added (final concentration 10 mM). Nucleotide loaded GSH sepharose bound GTPases were added to pre-cleared lysates and incubated at 4°C rotating for 4 h. The beads were washed six times with wash buffer 1 (20 mM Tris–HCl pH 7.4, 150 mM NaCl, 2.5 mM $MgCl_2$, 0.2% Triton-X-100) and three times with wash buffer 2 (20 mM Tris–HCl pH 7.4, 2.5 mM $MgCl_2$). Bound proteins were eluted with sample buffer (63 mM Tris–HCl, pH 6.8, 2.5% SDS, 5% glycerol, 5% β-mercaptoethanol, 0.005% bromophenol blue) and binding of NOSTRIN to the small GTPases was analysed by immunoblotting.

Rac GTPase activation assay

Lysates of SFV-NOSTRIN, SFV-NOSTRIN-ΔSH3 or SFV-NOSTRIN-ΔHR1 expressing cells were prepared in PAK-CRIB lysis buffer (50 mM Tris–HCl pH 7.5, 200 mM NaCl, 10 mM $MgCl_2$, 5% Glycerol, 1% Triton-X-100, 1 mM PMSF, 10 μM Aprotinin, 1 mM Benzamidin). EDTA was added to the lysates (final concentration 24 μM). Lysates were incubated with GST-PAK-CRIB (20 μg) coupled to GSH sepharose for 40 min rotating at 4°C. Beads were washed three times with PAK wash buffer (25 mM Tris–HCl pH 7.5, 40 mM NaCl, 30 mM $MgCl_2$, 1 mM DTT, 1% NP-40) and two times with PAK wash buffer without detergent. Bound proteins were eluted with sample buffer. Precipitation of endogenous, active Rac1 was monitored by immunoblotting. Alternatively, Rac1 activity in MLECs was measured after 6 h of starvation in serum free medium and stimulation with 25 ng/ml FGF-2 (PeproTech) using the Active Rac1 pulldown and detection kit (Pierce Biotechnology) according to the manufacturer's instructions.

NOSTRIN-FGFR1 interaction analysis

For co-immunoprecipitiation HeLa cell lysates were prepared in lysis buffer (50 mM Tris–HCl pH 7.4, 150 mM NaCl, 2 mM EDTA, 1% NP-40, 25 mM NaF, 1 mM Na_3VO, supplemented with protease inhibitor cocktail (Roche)) and immunoprecipitation was performed using rabbit anti mouse NOSTRIN antiserum in combination with protein A/G-agarose (Santa Cruz). Precipitated proteins were analysed by immunoblotting. Co-immunoprecipitation from MLEC lysates was performed accordingly using rabbit anti-FGFR1 antibody (Santa Cruz, sc-121). For pulldown experiments NIH-3T3 cell lysates were prepared in lysis buffer (as above) and incubated with GSH-Sepharose beads (GE Healthcare) coupled with equal amounts of GST-tagged full size NOSTRIN or NOSTRIN deletion constructs. Subsequently beads were washed three times with the lysis buffer, boiled in sample buffer and binding of FGFR1 to NOSTRIN was analysed by immunoblotting. For direct interaction studies the C-terminal part of human FGFR1, encompassing aa692–822 was subcloned from RZPD full length cDNA clone no. IRAKp961I0214Q2 into pGEX4T1 vector, expressed as GST-fusion protein and released by thrombin cleavage. Equal amounts of the C-terminal part of FGFR1 were incubated with GST-NOSTRIN or GST-NOSTRIN deletion constructs coupled to GSH-Sepharose beads in incubation buffer (20 mM Tris pH 8.4, 150 mM NaCl, 2.5 mM $CaCl_2$, 10% Glycerol, 1% Triton-X-100, 1 mM DTT supplemented with protease inhibitor cocktail (Roche)). Finally Sepharose beads were washed three times with the incubation buffer and two times with PBS. Bound proteins were analysed by immunoblotting.

Immunoblotting and Immunohistochemistry

In this study 2 different NOSTRIN antibodies were used. (1) A monoclonal antibody raised in mouse against human NOSTRIN and described previously (Mookerjee *et al*, 2007). This was used for immunoblotting in Figures 4B–D, 5A, B and 6B (2) A polyclonal antiserum against mouse NOSTRIN was produced using recombinant GST-tagged NOSTRINaa337–506 purified from *E. coli* BL21 as antigen. Standard procedures were used for immunisation and bleeding of rabbits. This was used for immunoblotting in Figures 1D and 7A, B. Additional antibodies were directed against GAPDH (Abcam ab8245) Figure 7A; FGFR1 (polyclonal FGFR1-specific antiserum (Mohammadi *et al*, 1991) Figure 6B and C; FGFR1 (Santa Cruz sc-121) Figure 6D; GST (Amersham 27-4577-01) Figure 4B; His-Tag (Bethyl A190-114A) Figure 5E; Rac1 (BD Pharmingen 610650) Figures 5A, B and 7C; Sos1 (Santa Cruz sc-256) Figure 5C and D; Tiam1 (Santa Cruz sc-872); Vav2 (Acris AP220506); vinculin (Sigma v9131) Figure 1D. For immunohistochemistry an antibody directed against PECAM-1 was used (BD Pharmingen 553370) in combination with biotinylated goat anti-rat secondary antibody (BD Pharmingen).

Statistics

Data are expressed as the mean ± s.e.m., and statistical evaluation was performed by unpaired two-tailed *t*-test or two-way ANOVA with Bonferroni post tests by GraphPad Prism. Values of $P<0.05$ were considered statistically significant.

Ethical review

Zebrafish were maintained under standard conditions at the MPI for Heart and Lung Research, Bad Nauheim. Mice were maintained at the animal facility of the Goethe University Frankfurt, Medical School. All animal experiments were performed in compliance with the relevant laws and institutional guidelines and were approved by local animal ethics committees.

Supplementary data

Supplementary data are available at *The EMBO Journal* Online (http://www.embojournal.org).

Acknowledgements

We thank Dr Masood Siddique and Kristina Wagner for generation of the NOSTRIN antiserum, Prof Amparo Acker-Palmer and Dr Suphansa Sawamiphak for their introduction to MLEC isolation and Prof Ivan Dikic for critical reading and discussion of the manuscript. This work was supported by the German Research Foundation (SFB 834 IK and SO, TR-SFB 23/A6 JH, RP and IF and EXC 147 BJ), the Australian Research Council (DP110100389 ALM) and the Australian Zebrafish Phenomics Facility (NH&MRC APP455871 ACP).

Author contributions: IK, AS-I and SO designed the study, IK, AS-I, ACP, RP, BJ and SO designed experiments, IK, JH, A S-I, NO, BJ and AG performed experiments, IK, JH, AS-I, NO, RP, BJ, MH and SO analysed data, BJ provided transgenic fish lines, MH, ALM, IF and WM-E gave conceptual advice, IK, MH and SO wrote the manuscript.

Conflict of interest

The authors declare that they have no conflict of interest.

References

Abe K, Rossman KL, Liu B, Ritola KD, Chiang D, Campbell SL, Burridge K, Der CJ (2000) Vav2 is an activator of Cdc42, Rac1, and RhoA. *J Biol Chem* **275:** 10141–10149

Acevedo L, Yu J, Erdjument-Bromage H, Miao RQ, Kim JE, Fulton D, Tempst P, Strittmatter SM, Sessa WC (2004) A new role for Nogo as a regulator of vascular remodeling. *Nat Med* **10:** 382–388

Ahmed S, Goh WI, Bu W (2010) I-BAR domains, IRSp53 and filopodium formation. *Semin Cell Dev Biol* **21:** 350–356

Akimoto T, Hammerman MR (2003) Fibroblast growth factor 2 promotes microvessel formation from mouse embryonic aorta. *Am J Physiol Cell Physiol* **284:** C371–C377

Al-Shabrawey M, El-Remessy A, Gu X, Brooks SS, Hamed MS, Huang P, Caldwell RB (2003) Normal vascular development in mice deficient in endothelial NO synthase: possible role of neuronal NO synthase. *Mol Vis* **9:** 549–558

D'Amico G, Jones DT, Nye E, Sapienza K, Ramjuan AR, Reynolds LE, Robinson SD, Kostourou V, Martinez D, Aubyn D, Grose R, Thomas GJ, Spencer-Dene B, Zicha D, Davies D, Tybulewicz V, Hodivala-Dilke KM (2009) Regulation of lymphatic-blood vessel separation by endothelial Rac1. *Development* **136:** 4043–4053

Deng CX, Wynshaw-Boris A, Shen MM, Daugherty C, Ornitz DM, Leder P (1994) Murine FGFR-1 is required for early postimplantation growth and axial organization. *Genes Dev* **8:** 3045–3057

De Smet F, Segura I, De Bock K, Hohensinner PJ, Carmeliet P (2009) Mechanisms of vessel branching: filopodia on endothelial tip cells lead the way. *Arterioscler Thromb Vasc Biol* **29:** 639–649

Dormond O, Foletti A, Paroz C, Ruegg C (2001) NSAIDs inhibit alpha V beta 3 integrin-mediated and Cdc42/Rac-dependent endothelial-cell spreading, migration and angiogenesis. *Nat Med* **7:** 1041–1047

Elfenbein A, Rhodes JM, Meller J, Schwartz MA, Matsuda M, Simons M (2009) Suppression of RhoG activity is mediated by a syndecan 4-synectin-RhoGDI1 complex and is reversed by PKCalpha in a Rac1 activation pathway. *J Cell Biol* **186:** 75–83

Epting D, Wendik B, Bennewitz K, Dietz CT, Driever W, Kroll J (2010) The Rac1 regulator ELMO1 controls vascular morphogenesis in zebrafish. *Circ Res* **107:** 45–55

Feraud O, Cao Y, Vittet D (2001) Embryonic stem cell-derived embryoid bodies development in collagen gels recapitulates sprouting angiogenesis. *Lab Invest* **81:** 1669–1681

Frost A, Unger VM, De Camilli P (2009) The BAR domain superfamily: membrane-molding macromolecules. *Cell* **137:** 191–196

Gerhardt H, Betsholtz C (2005) How do endothelial cells orientate? *Exs*3–15

Gerhardt H, Golding M, Fruttiger M, Ruhrberg C, Lundkvist A, Abramsson A, Jeltsch M, Mitchell C, Alitalo K, Shima D, Betsholtz C (2003) VEGF guides angiogenic sprouting utilizing endothelial tip cell filopodia. *J Cell Biol* **161:** 1163–1177

Guerrier S, Coutinho-Budd J, Sassa T, Gresset A, Jordan NV, Chen K, Jin WL, Frost A, Polleux F (2009) The F-BAR domain of srGAP2 induces membrane protrusions required for neuronal migration and morphogenesis. *Cell* **138:** 990–1004

Heath RJ, Insall RH (2008) F-BAR domains: multifunctional regulators of membrane curvature. *J Cell Sci* **121:** 1951–1954

Ho HY, Rohatgi R, Lebensohn AM, Le M, Li J, Gygi SP, Kirschner MW (2004) Toca-1 mediates Cdc42-dependent actin nucleation by activating the N-WASP-WIP complex. *Cell* **118:** 203–216

Horowitz A, Simons M (2008) Branching morphogenesis. *Circ Res* **103:** 784–795

Hu J, Troglio F, Mukhopadhyay A, Everingham S, Kwok E, Scita G, Craig AW (2009) F-BAR-containing adaptor CIP4 localizes to early endosomes and regulates Epidermal Growth Factor Receptor trafficking and downregulation. *Cell Signal* **21:** 1686–1697

Icking A, Matt S, Opitz N, Wiesenthal A, Muller-Esterl W, Schilling K (2005) NOSTRIN functions as a homotrimeric adaptor protein facilitating internalization of eNOS. *J Cell Sci* **118:** 5059–5069

Icking A, Schilling K, Wiesenthal A, Opitz N, Muller-Esterl W (2006) FCH/Cdc15 domain determines distinct subcellular localization of NOSTRIN. *FEBS Lett* **580:** 223–228

Jakobsson L, Franco CA, Bentley K, Collins RT, Ponsioen B, Aspalter IM, Rosewell I, Busse M, Thurston G, Medvinsky A, Schulte-Merker S, Gerhardt H (2010) Endothelial cells dynamically compete for the tip cell position during angiogenic sprouting. *Nat Cell Biol* **12:** 943–953

Javerzat S, Auguste P, Bikfalvi A (2002) The role of fibroblast growth factors in vascular development. *Trends Mol Med* **8:** 483–489

Jin SW, Beis D, Mitchell T, Chen JN, Stainier DY (2005) Cellular and molecular analyses of vascular tube and lumen formation in zebrafish. *Development* **132:** 5199–5209

Koduru S, Kumar L, Massaad MJ, Ramesh N, Le Bras S, Ozcan E, Oyoshi MK, Kaku M, Fujiwara Y, Kremer L, King S, Fuhlbrigge R, Rodig S, Sage P, Carman C, Alcaide P, Luscinskas FW, Geha RS (2010) Cdc42 interacting protein 4 (CIP4) is essential for integrin-dependent T-cell trafficking. *Proc Natl Acad Sci USA* **107:** 16252–16256

Landgren E, Klint P, Yokote K, Claesson-Welsh L (1998) Fibroblast growth factor receptor-1 mediates chemotaxis independently of direct SH2-domain protein binding. *Oncogene* **17:** 283–291

Larrivee B, Freitas C, Suchting S, Brunet I, Eichmann A (2009) Guidance of vascular development: lessons from the nervous system. *Circ Res* **104:** 428–441

Lawson ND, Weinstein BM (2002) In vivo imaging of embryonic vascular development using transgenic zebrafish. *Dev Biol* **248:** 307–318

Magnusson P, Rolny C, Jakobsson L, Wikner C, Wu Y, Hicklin DJ, Claesson-Welsh L (2004) Deregulation of Flk-1/vascular endothelial growth factor receptor-2 in fibroblast growth factor receptor-1-deficient vascular stem cell development. *J Cell Sci* **117:** 1513–1523

Magnusson PU, Dimberg A, Mellberg S, Lukinius A, Claesson-Welsh L (2007) FGFR-1 regulates angiogenesis through cytokines interleukin-4 and pleiotrophin. *Blood* **110:** 4214–4222

Magnusson PU, Ronca R, Dell'Era P, Carlstedt P, Jakobsson L, Partanen J, Dimberg A, Claesson-Welsh L (2005) Fibroblast growth factor receptor-1 expression is required for hematopoietic but not endothelial cell development. *Arterioscler Thromb Vasc Biol* **25:** 944–949

McCormick ME, Goel R, Fulton D, Oess S, Newman D, Tzima E (2011) Platelet-endothelial cell adhesion molecule-1 regulates endothelial NO synthase activity and localization through signal transducers and activators of transcription 3-dependent NOSTRIN expression. *Arterioscler Thromb Vasc Biol* **31:** 643–649

Michiels F, Habets GG, Stam JC, van der Kammen RA, Collard JG (1995) A role for Rac in Tiam1-induced membrane ruffling and invasion. *Nature* **375:** 338–340

Mohammadi M, Honegger AM, Rotin D, Fischer R, Bellot F, Li W, Dionne CA, Jaye M, Rubinstein M, Schlessinger J (1991) A tyrosine-phosphorylated carboxy-terminal peptide of the fibroblast growth factor receptor (Flg) is a binding site for the SH2 domain of phospholipase C-gamma 1. *Mol Cell Biol* **11:** 5068–5078

Mookerjee RP, Wiesenthal A, Icking A, Hodges SJ, Davies NA, Schilling K, Sen S, Williams R, Novelli M, Muller-Esterl W, Jalan R (2007) Increased gene and protein expression of the novel eNOS regulatory protein NOSTRIN and a variant in alcoholic hepatitis. *Gastroenterology* **132:** 2533–2541

Nicoli S, De Sena G, Presta M (2009) Fibroblast growth factor 2-induced angiogenesis in zebrafish: the zebrafish yolk membrane (ZFYM) angiogenesis assay. *J Cell Mol Med* **13:** 2061–2068

North TE, Goessling W, Peeters M, Li P, Ceol C, Lord AM, Weber GJ, Harris J, Cutting CC, Huang P, Dzierzak E, Zon LI (2009) Hematopoietic stem cell development is dependent on blood flow. *Cell* **137:** 736–748

Oess S, Icking A, Fulton D, Govers R, Muller-Esterl W (2006) Subcellular targeting and trafficking of nitric oxide synthases. *Biochem J* **396:** 401–409

Presta M, Dell'Era P, Mitola S, Moroni E, Ronca R, Rusnati M (2005) Fibroblast growth factor/fibroblast growth factor receptor system in angiogenesis. *Cytokine Growth Factor Rev* **16:** 159–178

Qualmann B, Koch D, Kessels MM (2011) Let's go bananas: revisiting the endocytic BAR code. *Embo J* **30:** 3501–3515

Roberts-Galbraith RH, Gould KL (2010) Setting the F-BAR: functions and regulation of the F-BAR protein family. *Cell Cycle* **9:** 4091–4097

Rousseau B, Larrieu-Lahargue F, Bikfalvi A, Javerzat S (2003) Involvement of fibroblast growth factors in choroidal angiogenesis and retinal vascularization. *Exp Eye Res* **77:** 147–156

Rozakis-Adcock M, Fernley R, Wade J, Pawson T, Bowtell D (1993) The SH2 and SH3 domains of mammalian Grb2 couple the EGF receptor to the Ras activator mSos1. *Nature* **363:** 83–85

Sawamiphak S, Seidel S, Essmann CL, Wilkinson GA, Pitulescu ME, Acker T, Acker-Palmer A (2010) Ephrin-B2 regulates VEGFR2 function in developmental and tumour angiogenesis. *Nature* **465:** 487–491

Schilling K, Opitz N, Wiesenthal A, Oess S, Tikkanen R, Muller-Esterl W, Icking A (2006) Translocation of endothelial nitric-oxide synthase involves a ternary complex with caveolin-1 and NOSTRIN. *Mol Biol Cell* **17:** 3870–3880

Sheikh F, Sontag DP, Fandrich RR, Kardami E, Cattini PA (2001) Overexpression of FGF-2 increases cardiac myocyte viability after injury in isolated mouse hearts. *Am J Physiol Heart Circ Physiol* **280:** H1039–H1050

Sini P, Cannas A, Koleske AJ, Di Fiore PP, Scita G (2004) Abl-dependent tyrosine phosphorylation of Sos-1 mediates growth-factor-induced Rac activation. *Nat Cell Biol* **6:** 268–274

Suchting S, Bicknell R, Eichmann A (2006) Neuronal clues to vascular guidance. *Exp Cell Res* **312:** 668–675

Suetsugu S, Toyooka K, Senju Y (2010) Subcellular membrane curvature mediated by the BAR domain superfamily proteins. *Semin Cell Dev Biol* **21:** 340–349

Tan W, Palmby TR, Gavard J, Amornphimoltham P, Zheng Y, Gutkind JS (2008) An essential role for Rac1 in endothelial cell function and vascular development. *Faseb J* **22:** 1829–1838

Toguchi M, Richnau N, Ruusala A, Aspenstrom P (2010) Members of the CIP4 family of proteins participate in the regulation of platelet-derived growth factor receptor-beta-dependent actin reorganization and migration. *Biol Cell* **102:** 215–230

Tomanek RJ, Christensen LP, Simons M, Murakami M, Zheng W, Schatteman GC (2010) Embryonic coronary vasculogenesis and angiogenesis are regulated by interactions between multiple FGFs and VEGF and are influenced by mesenchymal stem cells. *Dev Dyn* **239:** 3182–3191

Tomanek RJ, Sandra A, Zheng W, Brock T, Bjercke RJ, Holifield JS (2001) Vascular endothelial growth factor and basic fibroblast growth factor differentially modulate early postnatal coronary angiogenesis. *Circ Res* **88:** 1135–1141

Tzima E (2006) Role of small GTPases in endothelial cytoskeletal dynamics and the shear stress response. *Circ Res* **98:** 176–185

Wang Y, Nakayama M, Pitulescu ME, Schmidt TS, Bochenek ML, Sakakibara A, Adams S, Davy A, Deutsch U, Luthi U, Barberis A, Benjamin LE, Makinen T, Nobes CD, Adams RH (2010) Ephrin-B2 controls VEGF-induced angiogenesis and lymphangiogenesis. *Nature* **465:** 483–486

Woad KJ, Hunter MG, Mann GE, Laird M, Hammond AJ, Robinson RS (2012) Fibroblast growth factor 2 is a key determinant of vascular sprouting during bovine luteal angiogenesis. *Reproduction* **143:** 35–43

Yu PC, Gu SY, Bu JW, Du JL (2010) TRPC1 is essential for in vivo angiogenesis in zebrafish. *Circ Res* **106:** 1221–1232

Zhao B, Chun C, Liu Z, Horswill MA, Pramanik K, Wilkinson GA, Ramchandran R, Miao RQ (2010) Nogo-B receptor is essential for angiogenesis in zebrafish via Akt pathway. *Blood* **116:** 5423–5433

Zhao H, Pykalainen A, Lappalainen P (2011) I-BAR domain proteins: linking actin and plasma membrane dynamics. *Curr Opin Cell Biol* **23:** 14–21

Zimmermann K, Opitz N, Dedio J, Renne C, Muller-Esterl W, Oess S (2002) NOSTRIN: a protein modulating nitric oxide release and subcellular distribution of endothelial nitric oxide synthase. *Proc Natl Acad Sci USA* **99:** 17167–17172

